ANNALS OF GEOPHYSICS, 66, 2, SE216, 2023, doi:10.4401/ag-8839
OPEN ACCESS

Upper Mantle Anisotropy beneath Northern Algeria from Shear-Wave Splitting

Zohir Radi[*,1], Abdelkarim Yelles Chaouche[1], Salim Guettouche[1], Gotz Bokelmann[2]

(1) Center of Research in Astronomy Astrophysics and Geophysics, POB 63 Observatory Road, Algiers Algeria
(2) Institute for Meteorology and Geophysics, University of Vienna

Article history: received May 4, 2022; accepted September 27, 2022

Abstract

Northern Algeria is a large region in the north-western of Africa, lying on the collision boundary between the African and Eurasian plates. Few studies on Lithosphere and Mantle deformation have been conducted in this region. To better understand the seismic anisotropy patterns beneath this area, we used data from 17 broadband stations installed in Tellian and the Saharan atlases using the SKS shear wave splitting method by processing hundreds of teleseismic events. To estimate the seismic anisotropy, two parameters were calculated, the fast polarization direction and the delay time for each station-event pair. The results show that the seismic anisotropy can be described by two main orientations, ENE-WSW follows the general trend of the Saharan Atlas, particularly in the central and western parts, and ESE-WNW follows the Hodna Mountains in south-eastern Algeria. Our results show that the anisotropy can be explained by single and heterogeneity in the anisotropic structure, where the measurements are very scattered, and the delay time and fast direction changed with the events backazimuth. In the ABSD, CBBR and CDCN stations, which lie in the arc between the Sahara Atlas and the Aurès Mountains, the origin hypothesis of the seismic anisotropy can be linked to the existence of a detached slab. Moreover, in ABZH, OKGL and EARB stations located in the Kabylide and Western regions, it can be associated with the Gibraltar slab. Both slabs sinking in the African margin mantle were previously imaged by seismic tomography. For the remaining stations, the single-layer best explains the observed seismic anisotropy from their regular fast polarization direction. The comparison of the obtained fast directions with GPS measurements shows that anisotropy fast axes are nearly perpendicular to the convergence direction between the African and Eurasia plates.

Keywords: Shear wave splitting; SKS shear wave; Seismic anisotropy; Geodynamic; Northern Algeria

1. Introduction

Seismic anisotropy analysis is a key tool for determining the deformation state of the lithosphere and asthenosphere's deep layers. Structures with layered material [Backus, 1962] or fluid-filled rock cracks can cause seismic anisotropy on a macroscopic scale [Crampin, 1984; Kendall et al., 2006]. Minerals can be intrinsically anisotropic at the crystal scale. Olivine, for example, a major component of the mantle (60 to 70%), is strongly

anisotropic (18% on shear wave velocity; Mainprice, 2007). Seismic anisotropy is caused by the preferred orientation of anisotropic minerals in the mantle [Christensen and Crosson, 1968].

Seismic anisotropy derived from SKS wave splitting is an efficient tool for understanding Earth's upper mantle deformation [Silver and Chan, 1991; Levin et al., 2008; Bokelmann et al., 2013; Liu et al., 2020]. When shear waves pass through an anisotropic medium, they split into two waves that vibrate on orthogonal planes; one propagating faster than the other. The delay time (δt) is the difference in arrival time between them. This parameter aids in determining the depth and strength of the deformation while the polarization direction (this plane orientation with respect to the geographic North is called fast direction φ°) of the fast shear wave defines the deformation pattern. The purpose of this study is to analyze seismic anisotropy by computing φ° and δt from a teleseismic dataset (epicentral distance greater than 85°) with magnitude ≥ 5.5 recorded by Broad-Band (BB) stations deployed over northern Algeria. To accomplish this, we use SplitLab package of Wüstfeld et al. [2008] which includes three computational methods: rotation–correlation (RC) [Bowman and Ando, 1987], minimum energy (SC) [Silver and Chan, 1991], and the eigenvalue method (EV) [Silver and Chan, 1991].

Northern Algeria is known as a large deformation zone in north-western Africa, represented by the "Maghrebides Alpine chain," at the boundary between the Eurasian and African plates. It represents a key area to better understand the geodynamic evolution of the Alboran Basin and the Calabria subduction zones [e.g., Jolivet et al., 2008; Lucente et al., 2006]. The first seismic anisotropy study in Algeria was conducted by Barruol et al. [1999], followed by Schmid et al. [2004], based on a single BB station in Tamanrasset (Southern Algeria) and another in the Guelma region (Northern Algeria). Radi et al. [2015] investigated seismic anisotropy from SKS shear waves splitting over North-eastern Algeria, and used Rayleigh wave dispersion analysis to determine the crust and upper mantle shear wave structure [Radi et al., 2017; Radi and Yelles, 2022].

By using the SKS shear-waves splitting method on the 12 BB seismic stations installed in the central and north-western regions, we complete the seismic anisotropy analysis in Algeria. The obtained results are compared to velocity directions estimated from GPS measurements of the ten years of continuous data collected by the Algerian REGAT network, and we discuss and suggest geodynamic scenarios from earlier investigations.

2. Geodynamic setting

Over the last 30-35 Ma, the Mediterranean region's geodynamic evolution was powered by a subduction process, with, today, a slow convergence rate varying from west to east, between 5 mm/year to approximately 8 mm/year [Calais et al., 2003; Argus et al., 2011; DeMets et al., 2015; Altamimi et al., 2017] (Figure 1). Because it contains a large portion of the Maghrebides Alpine chain, stretching from Calabria to Gibraltar, northern Algeria is an important witness to this evolution [Wildi, 1983] (Figure 1).

The seismic risk in northern Algeria ranges from moderate to high [e.g., Layadi et al., 2016]. From north to south, the geological units are as follows: the internal domain of the Kabylides; the Tell system (also known as the External Tell); the Atlas system, which includes the High Plateaus, Saharan Atlas, and Aurès; and the Saharan platform [Bracène et al., 2002] (Figure 1).

Northern Algeria sufferd a number of geodynamic phases. The convergence of the early Paleocene and Villafranchian periods was the most significant. Beginning with the main Cenozoic convergence phase (Paleogene to present), the various geological domains experienced compression and distension from NE-SW to NW-SE. The Aurès Mountains, for example, experienced NE-SW distension from the Oligocene to the early Miocene, followed by Tortonian NW-SE compression and Pliocene NE-SW extension. From the early Paleocene to the late Eocene, NW-SE compression influenced the Saharan Atlas [Bracène et al., 2002].

3. Data and analysis methods

Following the May 21, 2003 earthquake in Boumerdès, Centre of Research in Astronomy Astrophysics and Geophysics (CRAAG) decided to establish the first Algerian Digital Seismological Network (ADSN) [Yelles-Chaouche et al., 2013]. Now, this network contains 17 broadband (BB) stations (Figure 2a). The BB stations have two types of digitizers: "Geodevice EDAS-24IP" coupled with "Geodevice BBVS-60s" sensors, and "Q330" equipped with "Streckeisen STS-2" sensors.

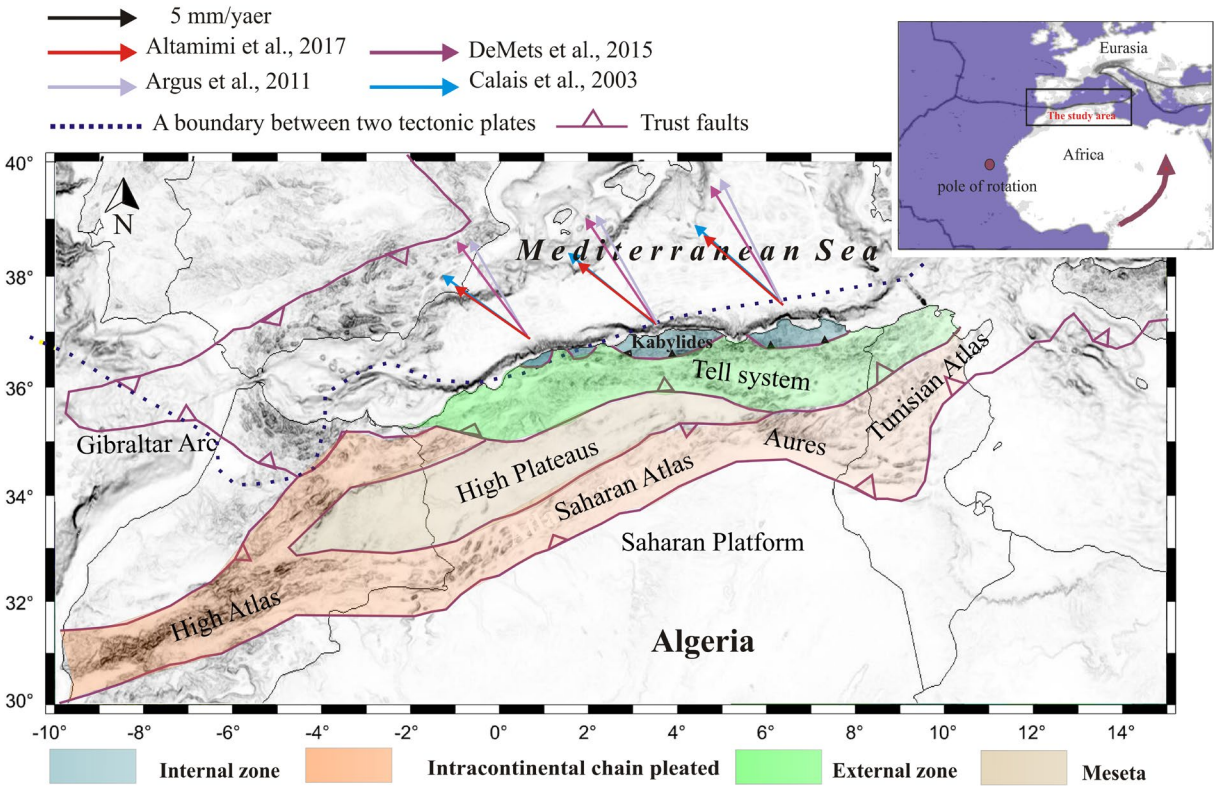

Figure 1. Map representing the main geological units of Northern Algeria inspired from Bracène et al. [2002], and the predicted velocities with directions along the Eurasia–African Plate boundary from different studies. In caption the RPM of African plate.

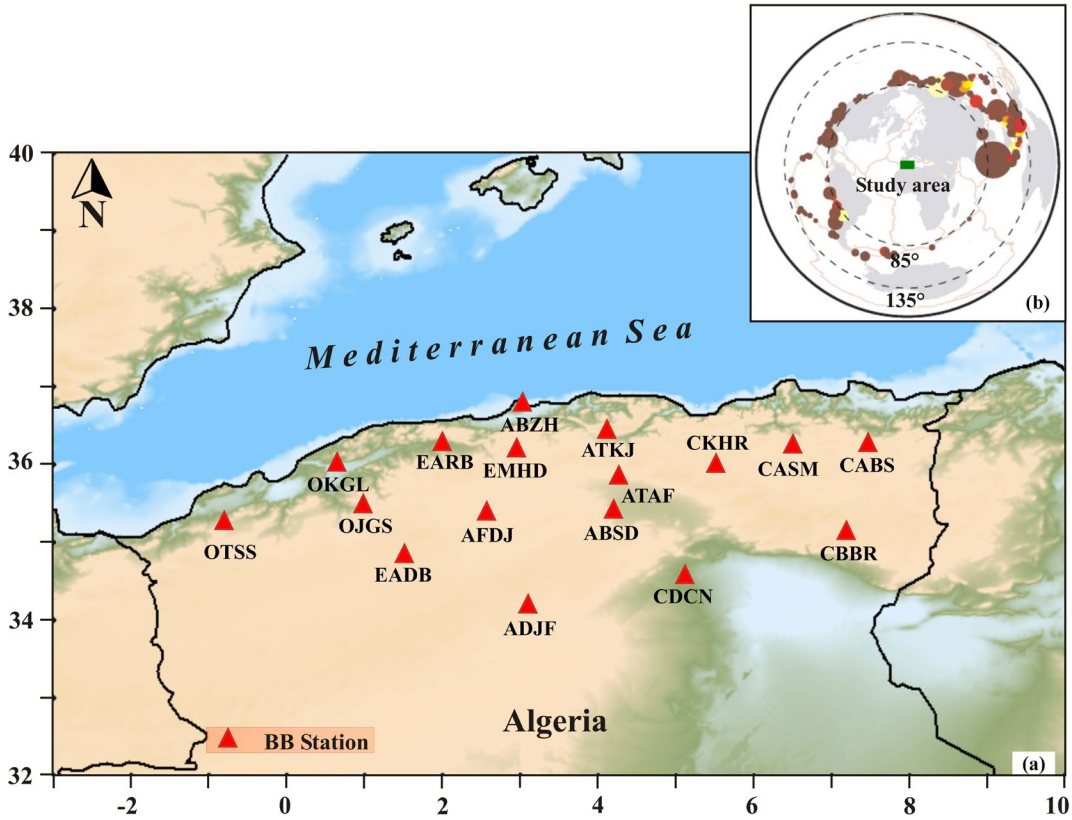

Figure 2. (a) Geographic distribution of permanent broadband stations of the Algerian Seismic Network in North Algeria; (b) Spatial distribution of earthquakes (Mw >5.5) used in the present study.

In this study, we examined over 1500 teleseismic events recorded by the 17 BB stations from 2010 to 2021, where the origin time and location were obtained from the National Earthquake Information Center (NEIC) or the Global Catalog CMT (Centroid Moment Tensor). To measure seismic anisotropy from SKS shear waves, the considered events' epicentral distance (Δ) must be greater than 85° and their magnitude Mw greater than 5.5. The distribution of teleseismic events used in this study as a function of depth, distance, and azimuth is plotted in Figure 2b.

An SKS wave crossing an anisotropic medium, is split into two waves polarised along two perpendicular planes and moving at different velocities. The delay time between the two waves will increase as they travel through the anisotropic medium. This technique aims to determine the orientation φ of the fast polarised wave's plane relative to the angle the polarized wave has respect to the North as well as the delay time, δt, between the two polarized waves from ground movement recording. The considered principle is to test various pairs of parameters (φ, δt) and quantify the correlation of the waveform between the two split waves [Silver and Chan, 1991]. We used the software called SplitLab [Wüstefeld, 2007; Wüstefeld et al., 2008]. This software programmed under Matlab language, allows us to manage data requests, creates an event database, and uses three different methods of anisotropy analysis: the Rotation/Correlation method [Bowman and Ando, 1987], the energy minimization on the transverse component, and Eigenvalues method [Silver and Chan, 1991]. A frequency filter is applied to our data between 0.02–1 Hz since this pass band includes the dominant period of SKS [Zhao et al., 2007].

Figure 3 shows an example of application of the different methods where splitting parameters are very consistent regardless of the used technique. The comparison of the three method's results can help to characterize individual splitting measurements as well as distinguish null observations from real splitting cases [Wüstefeld and Bokelmann, 2007]. When the SKS phase is not split, one obtains a so-called "null measurement", which can be explained by either the absence of anisotropy or an initial shear-wave polarisation parallel to the fast or slow polarisation orientation in the anisotropic layer [e.g., Silver and Chan, 1991; Wüstefeld and Bokelmann, 2007]. The SplitLab software assigns a quality factor, good, fair, or poor to shear-wave splitting measurements based on Wüstefeld and Bokelmann's criteria [2007]. These criteria differ slightly from those proposed by Barruol et al. [1997].

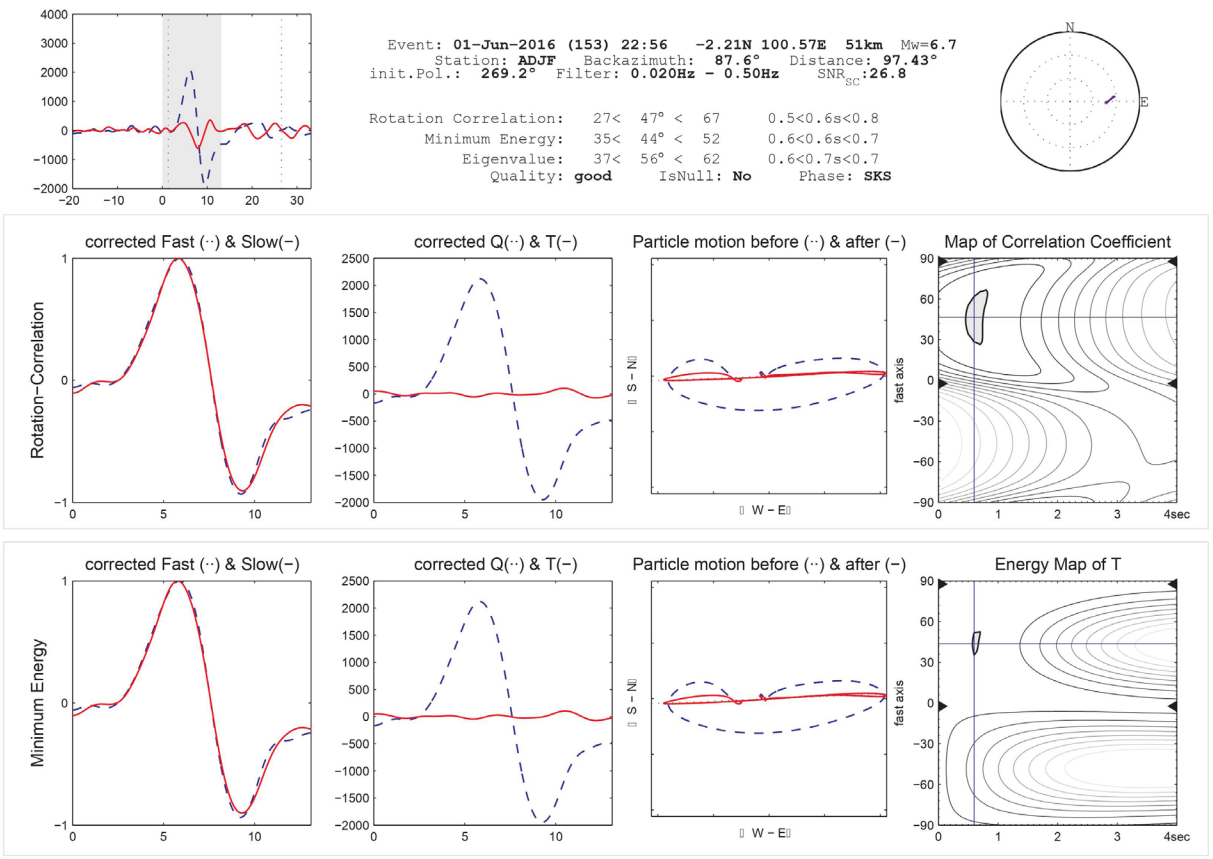

Figure 3. Example of processing results from the different computational methods used for an event occurred in Asia on June 01, 2016 with magnitude 6.7, recorded at ADJF station (epicentral distance = 90.43°).

This method was qualified using the following criteria: seismogram quality, SNR, energy on the transverse component, correlation of the two split waveforms, and elliptical particle motion before anisotropy correction and linearization after correction. After analyzing hundreds of teleseismic events recorded by BB, we found four groups of quality results: excellent (SNR>5), good, fair and poor, using the two criteria of Wüstefeld and Bokelmann [2007] and Barruol et al. [1997]. However, we considered only good and excellent measurements given in Table 1.

Station	lat	long	Event	Distance	Backazimuth	φ_{RC}	δt_{RC} (s)	φ_{SC}	δt_{SC} (s)	Quality
CABS	36.468	7.784	2010.070	102.44	236.4	-78<-64<-53	0.8<1.2<1.5	-66<-66<-43	0.4<1.2<2.6	fair
			2010.073	94.34	34.9	52<63<83	0.9<1.3<1.7	54<61<76	0.9<1.4<1.8	good
CKHR	36.016	5.510	2010.073	95.94	33.2	71<77<85	0.6<0.6<0.7	68<81<92	0.5<0.6<0.8	excellent
			2010.074	102.24	234.3	-90<-80<-71	0.8<1.1<1.4	-92<-80<-70	0.9<1.3<1.6	good
			2010.193	90.40	242.4	-97<-71<-50	0.3<0.6<0.9	-88<-62<-48	0.4<0.6<1.0	excellent
			2011.070	95.09	35.7	79<89<97	0.9<1.1<1.3	80<90<-86	0.9<1.1<1.3	good
			2011.204	95.14	32.3	58<81<105	0.4<0.6<1.0	60<86<104	0.4<0.7<1.1	excellent
			2011.242	119.22	75.6	-76<-66<-57	0.4<0.8<1.0	-92<-68<-37	0.4<0.8<1.3	excellent
CDCN	34.586	5.119	2013.102	96.53	39.7	10<24<34	1.2<1.7<2.0	-19<6<21	0.8<1.3<1.9	excellent
			2013.183	88.62	85.2	2<16<26	1.4<1.7<1.9	13<17<21	1.4<1.6<1.9	excellent
			2013.329	94.05	23.2	-43<-25<-13	2.4<2.7<3.0	-37<-29<-2.7	2.4<2.7<3.0	fair
			2020.270	85.97	162.5	-54<-42<-32	0.7<1.0<1.4	-98<-55<-25	0.2<0.8<1.7	fair
			2021.223	111.38	65.3	20<27<36	0.7<0.8<1.0	3<17<31	0.6<0.8<1.0	good
			2021.224	95.64	195.8	74<89<110	3.1<2.8<4.0	68<80<88	2.7<2.8<4.0	good
CBBR	35.144	7.191	2011.081	97.23	33.3	47<62<80	1.0<1.4<1.8	52<69<-84	0.8<1.4<1.9	fair
			2011.234	99.23	91.4	-61<-49<-37	0.5<0.6<0.8	-64<-47<-31	0.4<0.6<0.8	fair
			2011.327	96.01	34.9	62<73<87	1.6<1.9<2.2	68<83<98	1.4<2.2<2.9	fair
			2012.087	94.26	33.0	-88<-87<-82	1.2<1.6<2.0	-84<-77<-76	1.6<2.0<2.4	excellent
			2013.243	93.48	1.3	-57<-47<-39	0.3<0.5<0.6	-62<-33<-17	0.3<0.5<0.8	fair
			2021.223	109.59	66.5	-60<-50<-42	3.6<3.8<4.0	-56<-45<-41	3.2<3.7<4.0	good
			2021.234	98.73	195.2	-59<-33<-11	0.3<0.6<1.0	-78<-27<1	0.4<0.7<1.6	good
			2021.236	91.21	20.6	81<84<89	1.8<2.0<2.1	-90<-85<-84	2.1<2.5<2.8	excellent
CASM	36.271	6.496	2012.319	97.99	239.5	64<70<79	1.6<1.9<2.1	70<78<92	1.1<1.7<2.2	good
			2013.109	90.09	18.1	71<79<88	1.0<1.2<1.3	72<76<82	0.9<1.1<1.3	excellent
			2013.109	91.52	23.8	62<70<79	0.5<0.6<0.7	72<88<94	0.5<0.7<1.0	good
			2013.167	91.09	293.8	72<81<91	1.5<1.8<2.1	76<82<88	1.7<1.8<2.6	good
			2013.277	100.03	131.0	-88<-81<-75	0.7<0.9<1.0	-80<-79<-66	0.5<0.8<1.2	good
			2013.288	105.40	65.0	8<17<27	0.5<0.8<1.1	-13<17<50	0.4<0.8<1.5	fair
			2021.234	99.67	194.9	19<31<50	1.0<1.6<2.4	19<35<90	0.6<1.6<3.4	good
			2021.236	90.35	20.2	38<46<66	0.6<1.0<1.3	33<54<84	0.7<1.1<1.4	good
ABZH	36.797	3.032	2015.052	97.72	27.6	75<79<85	0.3<1.1<1.3	-66<-66<-43	0.4<1.2<2.6	fair
			2015.260	94.85	234.4	52<64<76	0.7<1.1<1.5	54<72<92	0.8<1.2<1.7	good
			2020.270	88.6	161.3	-108<-74<-57	0.0<1.3<2.3	-70<-51<-40	0.0<1.4<1.6	fair
			2020.293	87.40	350.0	49<58<68	0.8<1.4<1.9	30<46<66	0.0<1.6<1.7	good
			2020.335	87.02	26.6	33<55<73	0.7<1.7<2.4	27<61<84	0.8<1.9<2.7	good
			2021.224	97.34	194.8	-72<-57<-43	2.1<2.6<3.1	-54<-45<-39	2.0<2.5<3.1	excellent
			2021.234	99.75	193.6	60<70<82	0.5<0.9<1.3	17<44<94	0.2<1.0<2.9	good
ATKJ	36.442	4.124	2015.051	95.13	30.02	75<85<95	1.1<1.5<1.8	70<84<98	1.5<1.6<2.1	excellent
			2015.052	95.08	30.1	74<82<90	0.9<1.2<1.4	56<64<78	1.1<1.4<1.8	good
			2015.150	103.80	38.9	74<84<95	0.3<0.6<0.9	64<75<88	0.6<0.7<1.0	excellent
			2016.014	93.01	29.05	72<82<93	0.5<0.7<0.8	46<67<98	0.7<1.1<1.9	good
			2016.153	96.57	87.09	56<66<76	0.7<1.0<1.2	60<70<76	0.9<1.1<1.3	excellent
			2021.234	99.36	193.9	57<86<100	1.0<1.5<2.1	78<88<92	1.3<1.6<1.9	excellent
			2021.236	90.83	18.7	46<63<84	0.1<0.5<1.0	49<59<77	0.0<0.7<0.9	good

Station	lat	long	Event	Distance	Backazimuth	φ_{RC}	δt_{RC} (s)	φ_{SC}	δt_{SC} (s)	Quality
			2010.113	102.29	232.4	32<37<43	1.5<1.6<1.8	27<32<41	1.2<1.6<2.0	good
			2010.139	86.38	261.1	32<39<48	1.6<1.8<2.0	39<43<50	1.7<1.9<2.1	excellent
ATAF	35.871	4.265	2010.151	83.06	81.3	-0.2<17<41	0.9<1.1<1.2	9<19<31	0.9<1.1<1.3	excellent
			2015.110	96.18	54.01	2<17<38	0.4<0.7<1.1	13<24<41	0.4<0.8<1.3	good
			2016.014	93.41	29.6	65<75<86	0.5<0.6<0.7	56<66<78	0.5<0.7<0.8	excellent
			2015.051	97.76	27.50	-80<-74<-48	0.0<0.4<1.0	-136<-70<-23	0.0<0.4<4.0	good
			2015.308	122.97	75.8	-102<-84<-68	1.4<1.8<2.1	-134<-86<-38	1.3<1.8<2.2	good
AFDJ	35.401	2.575	2016.031	98.47	234.3	-102<-86<-73	1.0<1.3<1.6	-96<-94<-90	1.3<1.5<1.7	good
			2020.322	96.65	88.7	-74<-65<57	3.0<3.3<3.6	-92<-69<-58	2.4<3.3<4.0	good
			2021.236	92.21	17.8	33<50<68	0.6<0.8<1.1	33<50<74	0.4<0.8<1.3	fair
			2015.047	94.93	197.7	46<59<73	0.5<1.0<1.4	35<86<98	0.5<1.5<4.0	good
			2016.301	99.46°	235.1°	27<66<93	1.6<2.5<3.3	68<79<102	1.7<2.6<3.3	excellent
ABSD	35.434	4.198	2020.270	87.01	162.0	11<34<54	0.8<1.6<2.4	-19<22<43	1.0<1.4<1.7	gd null
			2021.234	98.65	194.1	-10<36<77	0.0<1.3<3.7	03<24<-60	1.3<1.8<4.0	fair
			2016.153	97.43	87.6	27<47<52	0.5<0.6<0.8	35<44<52	0.5<0.6<0.7	excellent
			2016.211	116.31	40.2	-15<08<28	0.3<0.6<1.1	-31<16<29	0.3<0.7<1.2	excellent
ADJF	34.215	3.098	2020.336	92.70	354.8	37<43<55	0.0<0.4<0.6	30<33<44	0.0<0.5<07	good
			2020.349	88.23	241.9	10<18<28	0.0<0.2<0.3	08<14<20	0.0<0.2<0.4	good
			2020.355	96.18	29.6	-40<-15<10	0.0<0.5<1.3	10<12<17	0.0<0.9<1.1	good
			2015.110	97.39	52.6	-90<-89<-48	0.4<0.6<1.7	-70<-61<-48	0.4<0.8<1.7	good
			2016.014	93.91	28.2	55<80<108	0.3<0.7<1.0	43<52<70-	0.6<1.0<1.4	good
EARB	36.301	2.006	2016.211	115.25	38.6	73<80<89	0.4<0.6<0.8	80<-73<-60	0.3<0.9<2.0	good
			2016.301	98.65	234.1	15<26<36	0.8<1.3<1.6	13<26<41	0.8<1.3<1.8	excellent
			2010.113	101.65	231.8	48<56<64	1.2<1.4<1.6	60<64<72	1.3<1.4<1.5	excellent
			2010.144	85.52	254.2	-2<23<45	0.3<0.5<0.7	29<46<58	0.3<0.5<0.7	excellent
EMHD	36.209	2.950	2010.163	84.62	84.3	2<15<30	0.5<0.9<1.2	1<56<80	0.1<1.1<2.3	fair
			2016.014	93.63	28.8	38<45<55	1.3<1.5<1.6	46<53<62	1.0<1.4<1.8	excellent
			2016.211	114.84	39.4	60<71<83	0.2<0.3<0.5	37<73<100	0.2<0.4<0.8	good
			2016.014	95.35	27.9	-38<-11<15	0.0<0.2<0.5	-64<-52<11	0.1<0.8<3.1	fair
			2016.153	98.65	86.6	29<49<72	0.3<0.5<0.9	39<63<76	0.4<0.7<1.1	good
EADB	34.858	1.561	2020.336	91.94	353.8	34<45<59	0.3<0.4<0.6	11<40<68	0.3<0.4<0.7	excellent
			2021.234	97.33	192.6	46<73<97	0.5<0.9<1.4	56<81<-84	0.8<1.0<1.4	good
			2016.014	93.63	28.8	38<45<55	1.3<1.5<1.6	46<53<62	1.0<1.4<1.8	excellent
OTSS	35.281	0.793	2016.217	85.03	238.2	33<56<76	1.9<2.7<3.2	-11<30<50	0.7<2.2<3.6	good
			2010.116	100.70	52.1	-98<-82<-68	0.9<1.3<1.6	-84<-66<-54	0.8<1.4<2.1	good
			2010.139	85.53	258.9	63<71<79	1.4<1.7<1.9	58<65<72	1.1<1.5<2.0	good
			2010.163	86.49	83.0	19<29<41	0.1<0.3<0.5	9<39<64	0.3<0.6<0.9	good
OKGL	36.037	0.656	2010.169	127.15	60.9	-113<-86<-56	0.5<2.2<4.0	-100<-57<-39	1.2<2.3<4.0	good
			2013.021	91.45	82.8	-41<-30<-21	1.3<1.4<1.6	-74<-59<-50	1.6<2.0<2.5	fair
			2015.047	94.84	195.9	-90<-81<-60	0.0<1.6<1.7	-40<-44<-30	0.0<1.5<1.8	good
			2010.116	99.12	53.7	20<33<45	2.2<2.8<3.5	15<38<56	1.4<2.6<4.0	good
			2010.139	85.39	260.3	11<30<51	0.3<0.5<0.8	15<42<64	0.4<0.6<1.0	excellent
			2010.167	125.5	62.8	75<84<93	1.2<1.3<1.5	-92<-81<-76	1.0<1.3<1.6	fair
OJGS	35.505	0.990	2015.052	97.72	27.6	41<74<-68	0.6<1.2<1.8	39<70<100	0.4<1.1<1.8	good
			2015.260	94.85	234.4	52<64<76	0.7<1.1<1.5	54<72<88	0.8<1.2<1.7	good
			2021.234	97.87	192.4	39<51<65	0.2<0.5<0.9	19<52<84	0.1<0.6<1.3	excellent

Table 1. Shear-wave splitting parameter values obtained at each station (the values in blue are reported from Radi et al. [2015]; in black are the current calculated values).

4. Results

As mentioned in the previous section, for each teleseismic event, we used three calculation methods: rotation-correlation (RC), minimum energy (SC), and eigenvalue (EV) to compute the two shear-wave splitting parameters. The Table 1 presents the results of seismic anisotropy from east to west (the region is indicated by the first letter of the station name: "C" for east, "A" for middle, "E" for west-middle, and "O" for west). Because SC is a subset of the EV method, only RC and SC results are shown. Furthermore, the backazimuth range of good estimates for the SC technique is greater than for the RC technique. These differences in characteristics can be used to identify nulls in real-world datasets and assign a quality to the measurement [Wüstefeld et al., 2008]. The SC results were chosen to characterize upper mantle anisotropy, which is a commonly used term [Bokelmann et al., 2013; Qorbani et al.,

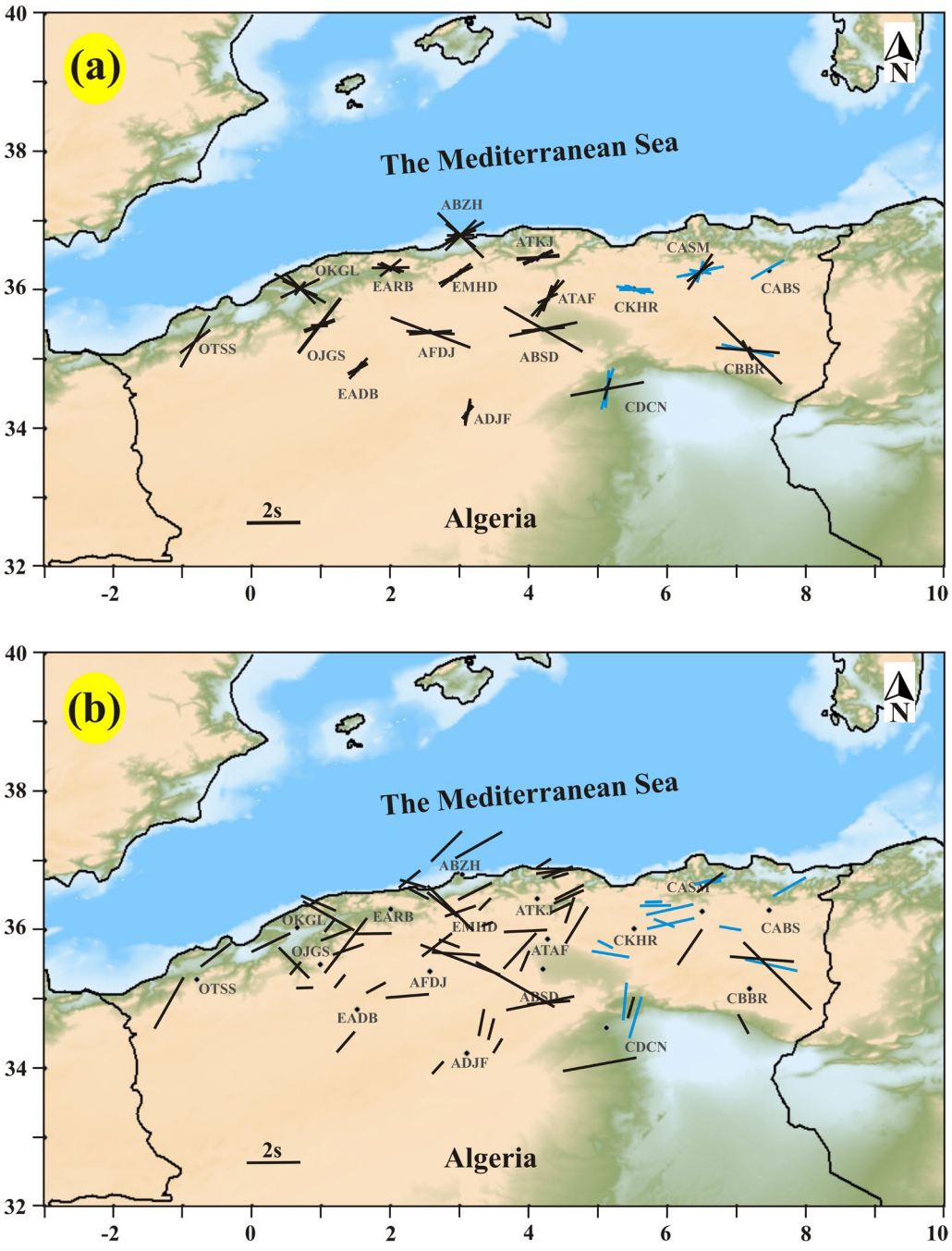

Figure 4. (a) Map showing individual fast orientations obtained from SKS analysis (good and excellent results) reported from Radi et al. [2015] (blue lines) and obtained in the present study (black line); (b) Map showing the individual fast orientations and projecting to a piercing depth of 100 km.

2015]. Figure 4a illustrates the results and in Table 1, older measurements for CABS, CASM, CBBR, CKHR, and CDCN stations from Radi et al. [2015] are marked in blue, while current measurements are marked in black.

The ABZH station in the middle of Algeria has only one excellent result with an orientation of -45° and a large delay time of 2.5 sec, and four good results with an orientation ranging from 44° to 72° and a delay time ranging from 1.0 to 1.9 sec (Table 1). ATKJ station, on the other hand, has four excellent results with a fast direction ranging from 70° to 88° and a delay time varying from 0.7 to 1.6 sec. There are three excellent results for ATAF station with $\varphi = 19°$, 43°, and 66° and delay times of 1.1, 1.9, and 0.7 sec, respectively, and three good results with $\varphi = 90°$, 24°, and 32° and delay times of 0.3, 0.8, and 1.6 sec. We only found good results for the AFDJ station, where the orientation ranges from -94 to -69° and the delay time varies from 0.4 to 3.3 secs.

For the western part, we found one excellent result with $\varphi = 40°$ at EADB station, with a delay time of 0.4 sec and five good results, when at EARB station, the excellent result is $\varphi = 26°$ and $\delta t = 1.3$ sec. There are three excellent results and one good at the EMHD station. We found a fast orientation $\varphi = 45°$ with a delay time of 1.4 sec for OTSS. There are only good results at OKGL station, and two excellent results and five good ones at OJGS station (Table 1).

In Table 2, we compute the mean of the fast orientation φ and the delay time δt using directional statistics formulas [Davis, 1986; Mardia and Jupp, 2000; Baccheschi et al., 2016], the concentration or spread of measurements at each station has represented by the circular average R of fast orientations and the length of the mean resultant.

Station	Lat (°N)	Long(°E)	φ °SC_{mean}	R	s (rad)	δt_{mean}(s)	$\Delta(\delta t)$
CABS	36.468	7.784	61			1.4	0.4
CKHR	36.016	5.510	97.68	0.891	0.56	0.85	±0.11
CDCN	34.586	5.119	22.25	0.594	0.50	1.6	±0.50
CBBR	35.144	7.191	124	0.728		2.22	±0.75
CASM	36.271	6.496	74.75	0.771	0.57	1.25	±0.15
ABZH	36.797	3.032	59.4	0.556	0.52	1.64	± 0.30
ATKJ	36.442	4.124	72.36	0.943	0.57	1.17	±0.12
ATAF	35.871	4.265	36.02	0.841	0.52	1.22	±0.24
AFDJ	35.401	2.575	100.3	0.932	0.50	1.75	±0.72
ABSD	35.434	4.198	67.37	0.567	0.38	2.05	±0.55
ADJF	34.215	3.098	23.54	0.906	0.52	0.58	±0.14
EARB	36.301	2.006	80.19	0.261	0.50	1.00	±0.12
EMHD	36.209	2.950	58.97	0.936	0.50	0.92	±0.25
EADB	34.858	1.561	61.49	0.835	0.45	0.82	±0.14
OTSS	35.281	0.793	41.5	0.92	0.38	1.80	±0.40
OKGL	36.037	0.656	105.85	0.347	0.52	1.46	±0.34
OJGS	35.505	0.990	54.72	0.883	0.52	1.22	±0.40

Table 2. Mean shear-wave splitting parameter values obtained for good and excellent quality at each station.

We used only the "good" and "excellent" results obtained with the minimum energy method, following the methodology of Barruol et al. [1999]. From Table 2, we observed R values close to one in the stations CABS, CASM, CKHR, ATAF, ATKJ, AFDJ, ADJF, EMHD, EADB, OTSS, and OJGS. As a result, these statins can be explained by only a single layer of seismic anisotropy. However, the remaining stations indicate the possibility of multiple anisotropic layers since the R is lower 0.7.

5. Discussion

To determine the relationship between our seismic anisotropy results and the geodynamic framework of northern Algeria, which has undergone a complex deformation evolution over geological time we looked at the mantle structure recently defined by seismic tomography for example Fichtner and Villaseor [2015], Hamai et al. [2018], Peral et al. [2022], and Radi and Yelles [2022]. The cited studies explain the origin of observed velocity anomalies in northern Algeria as slab traces or lithosphere tearing caused by an oceanic lithosphere subduction system into the African margin mantle. For this reason, the following sections discuss the seismic anisotropy results from individual measurements as well as the general trending of fast directions (Figure 4a). The results at each station are also shown by plotting the fast direction and projecting to a piercing depth of 100 km, which moves the points back along the ray path and gives a good overview of the seismic anisotropy parameters interpreted in Figure 4b. The discussion of our obtained results is organized from east to west.

The seismic anisotropy results of the CKHR, CABS, and CASM stations can be explained by a single layer of anisotropy related to measurements that are not widely scattered (Figure 4a). The delay time and fast direction are independent by event backazimuth (Figure 4b).

These stations' mean fast orientation and delay times are (-85°, 0.8 sec), (61°, 1.4 sec), and (68°, 1.2 sec), respectively, and are nearly parallel to the Tell system trend (Figure 1). The seismic anisotropy results at CBBR, CDCN, and ABSD stations are very scattered (Figure 4b), which is explained by the presence of heterogeneity in the anisotropic structure. One is thick and corresponds to (45°, 3.7 sec), (80°, 2.8 sec), and (79°, 2.6 sec), and can be related to the negative velocity anomaly centered in the north-east at 100 km from Radi and Yelles [2022] (Figure 5b), which may be caused by a failed subduction zone in this region, as supported by Spakman and Wortel [2004].

In the middle and western part of the study area, at ABZH station, we tentatively explain the structure beneath by the possibility of multiple anisotropic layers. The first layer has fast orientation and delay times of (72°, 1.2 sec), (46°, 1.6 sec), (61°, 1.9 sec), and (44°, 1.0 sec), and the second layer has (-45°, 2.5 sec), indicating likely 3D heterogeneities in that area of convergence [Bougrine et al., 2019], subduction [Hamai et al., 2018], and accretion [Spakman and Wortel, 2004]. For stations OKGL and EARB, the delay time and fast orientation are scattered indicating the presence of heterogeneity in the anisotropic structure. According to Civiero et al. [2019], the thick layer ($\delta t > 2$ sec) relates to the residual Gibraltar slab segment (below the eastern Rif in Morocco and the Baltics in the south-east of Spain) that is still connected to the surface or is in the process of detaching (Figure 5c).

The origin of seismic anisotropy can be explained by a single layer in the remaining stations, ATKJ, ATAF, ADJF, AFDJ, EMHD EADB, OJGS and OTSS from Figure 4a, because the delay time and fast orientation are not very scattered in each case separately. There is no greater backazimuth influence observed (Figure 4b).

In Figure 6, our obtained results of seismic anisotropy are plotted with displacement velocity directions from the GPS data of Bougrine et al. [2019]. The mean fast orientations from the single layer of seismic anisotropy (magenta line in Figure 6) are EW and NE-SW, and the displacement velocity directions from GPS data are NW-SE of Eurasia-Africa tectonic plate convergence. The fast orientations from the possibility of multiple anisotropic layers (brown line in Figure 6) are so scattered from one station to another, finding a correlation with displacement velocity directions is difficult.

GPS velocities and SKS splitting directions from the anisotropy reveal observations and information on the surface and upper mantle deformation. The relationship between the two directions shows coupling or decoupling deformation in the crust and upper mantle [e.g., Wang et al., 2008 Houlié and Stern, 2012]. Furthermore, the present study does not demonstrate the origin of multi-layers of seismic anisotropy from a geodynamic point of view. Analyzing the kind of deformation is open and will be more detailed in future scientific works.

In Figure 7, our SKS shear wave splitting results are plotted against those of database splitting from the Calabria arc to the Gibraltar arc [Diaz et al., 2010; Baccheschi et al., 2007, Lemnifi et al., 2015]. By adding, combining, and

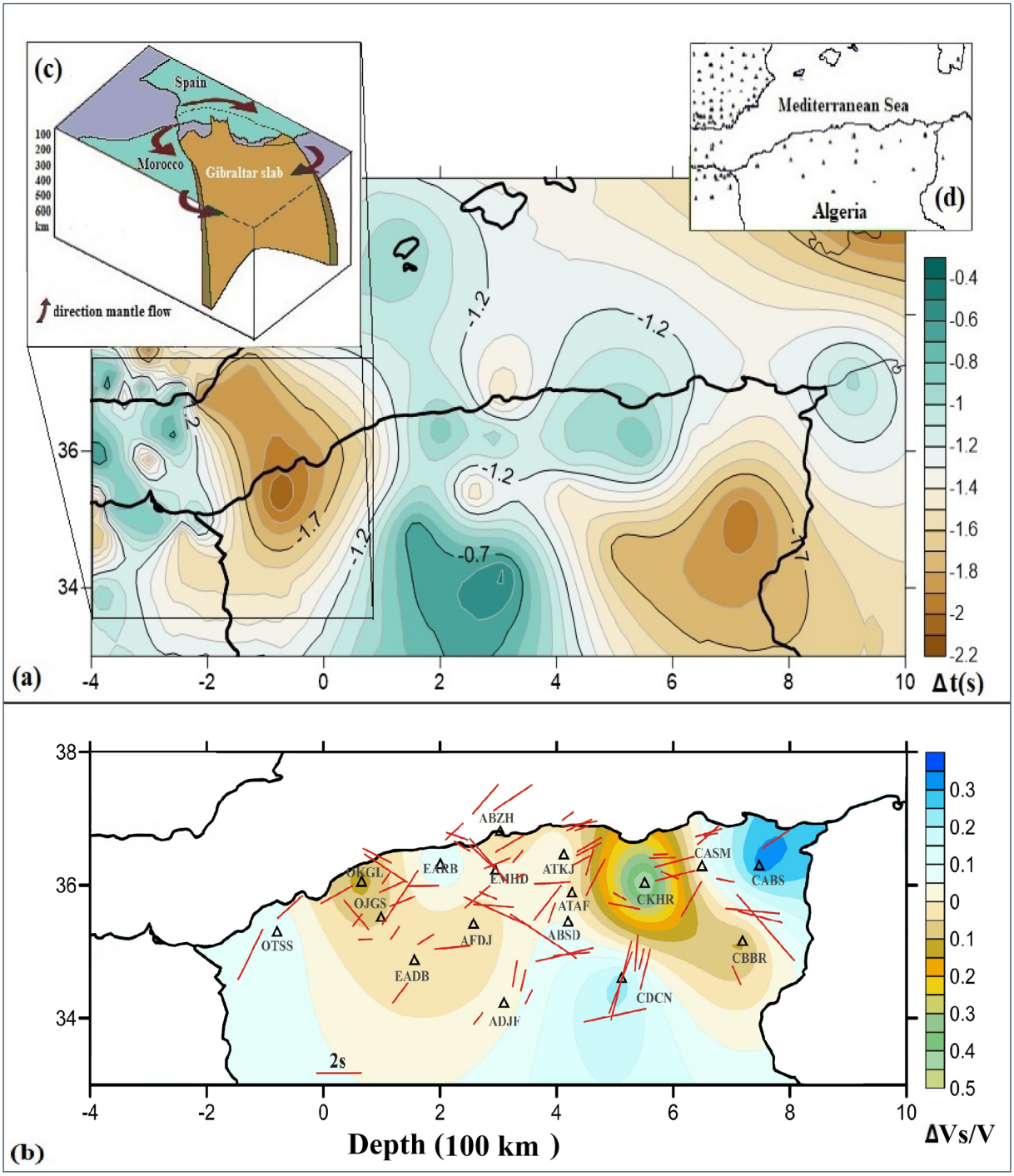

Figure 5. (a) Map showing delay time variation obtained by interpolation of collected data from SKS splitting database (https://doi.org/10.18715/sks_splitting_database) with our obtained results of the seismic network given in (d); (b) Relative Vs anomaly variations at 100 km depth modified from Radi and Yelles [2022] and tectonic interpretation with Gafsa (grey line with triangle) and offshore (red line with triangle) faults. (c) 3D Gibraltar slab presentation modified from Civiero et al. [2019].

visualizing all of these results, good reading and interpretation would be possible. We can see that the northwestern Mediterranean has had more seismic studies than North Algeria.

Figure 7 represents a similarity between fast orientation results in southern Tunisia and eastern Libya and results obtained for stations CDCN (for some individual measurements) and ADFJ stations, almost NS. Furthermore, the fast orientation of OTSS, OJGS, and EADB stations are comparable to that of stations installed in Morocco's eastern region (NE-SW).

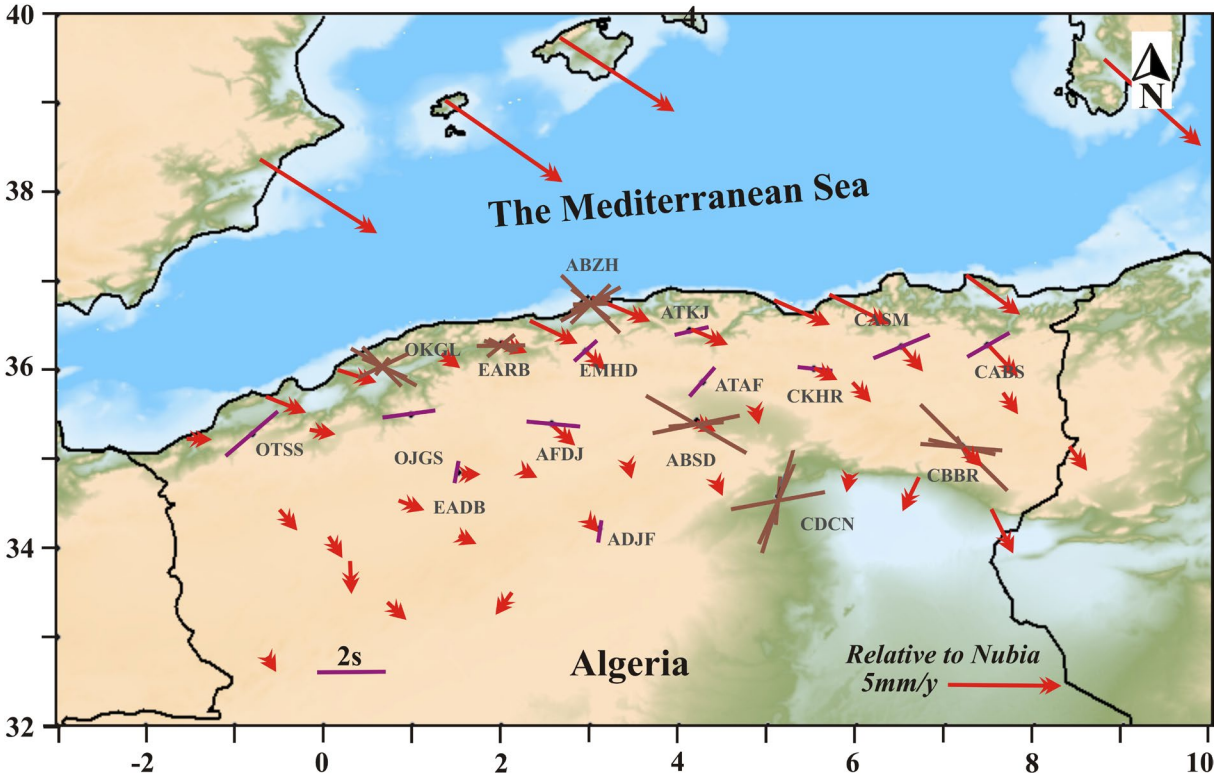

Figure 6. Map showing the fast orientations of SKS waves (magenta lines are the mean parameters, brown are individual measurements) compared to the GPS velocity directions with respect to Eurasia and Africa from Bougrine et al. (2019) (red arrows).

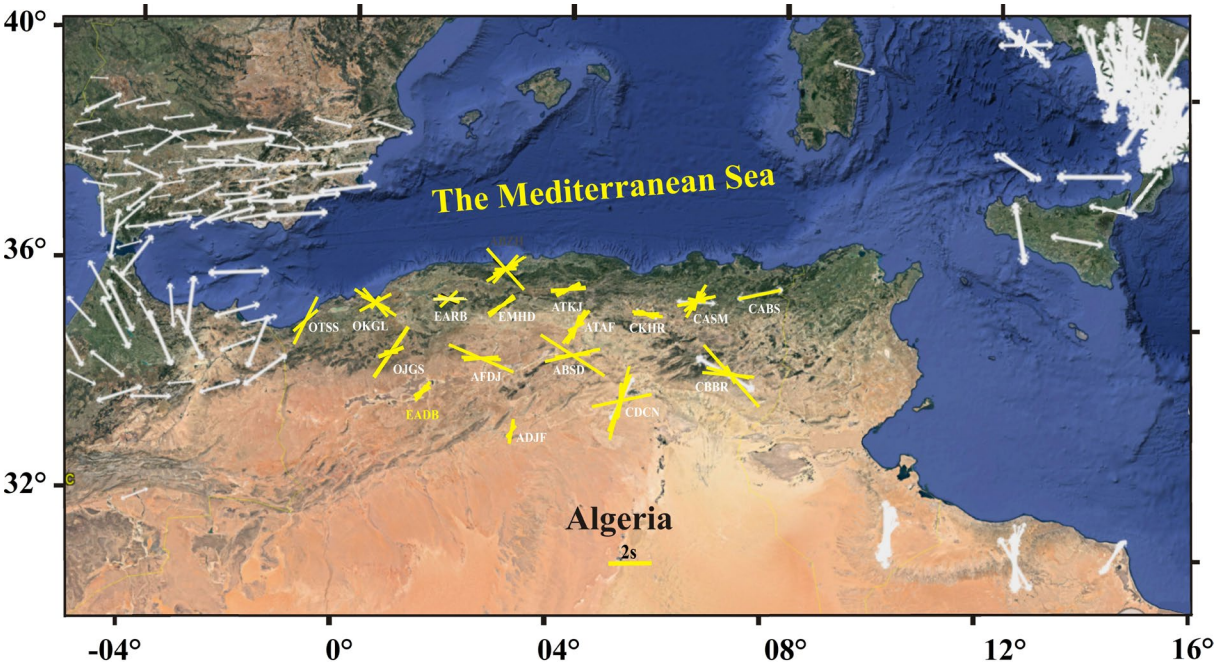

Figure 7. Map showing the fast orientations variations obtained from SKS splitting database between Gibraltar to Calabria Arcs (white double arrows) (https://doi.org/10.18715/sks_splitting_database) with our obtained results of this study (yellow lines).

6. Conclusion

We used the SplitLab package to determine the fast orientation and delay time of shear wave splitting parameters recorded at 17 permanent seismic stations in Northern Algeria. Our findings revealed that the complexity of splitting patterns varies by region. The single and two-layers can explain our seismic anisotropy results. Firstly, in a single layer interpretation, the measurements are not widely dispersed, and the delay time and fast direction do not vary with the backazimuth of the events (ADJF, AFDJ, ATAF, ATKJ, CABS, CASM, CKHR, EMHD, OTSS and OJGS stations). Secondly, the heterogeneity in the anisotropic structure of seismic anisotropy are for ABSD, CBBR, and CDCN stations situated in the arc between the Sahara Atlas and the Aurès Mountains (east region), ABZH in the Kabylide domain (middle of the study area), and OKGL, EARB stations situated in the western region. At ABZH, OKGL, and EARB stations, the origin of the thick layer is supported by the presence of the detached slab segment of the Gibraltar arc [Civiero et al., 2019; Peral et al., 2022]. Significant lateral variations in seismic anisotropy, particularly in fast polarisation orientations, have spatial scales comparable to those observed further west, in Morocco [Diaz et al., 2014]. The origin of the thick layer in the east (ABSD, CBBR, and CDCN) can be linked to the detached slab of Radi and Yelles [2022]. The anisotropy fast axes are nearly perpendicular to the GPS-measured convergence direction between the African and Eurasia plates. Our finding helps to explain the geodynamic evolution of these two parts of the western Mediterranean basin. As a result, the patterns are almost certainly linked to the larger pattern of larger-scale tectonics in the Western Mediterranean region. Nonetheless, this pattern indicates significant changes in this region, making Northern Algeria an interesting location for future research.

Acknowledgements. We would like to thank the CRAAG ADSN group for assisting with data acquisition, as well as the Constantine CRAAG regional service for helpful advice and comments. Also, many thanks to Khalissa Layadi for her assistance with this work. SplitLab was used to analyse the data [Wüstefeld et al., 2008]. We thank very much the Editor Professor Lucia Margheriti and the anonymous reviewers for the very relevant comments and suggestions which permit to enhance the quality of the paper. The datasets generated during the current study are not publicly available due to be not opened to the public yet, but are available from the corresponding author on reasonable request.

References

Altamimi, Z., L. Metivier, P. Rebischung, H. Rouby and X. Collilieux (2017). ITRF2014 plate motion model, J. Geophys. Res., 209, 1906–1912.

Argus, D., R. Gordon and C., DeMets (2011). Geologically current motion of 56 plates relative to the no–net–rotation reference frame, Geochem. Geophys. Geosyst., 12, Q11001.

Baccheschi, P., M. Pastori, L. Margheriti and D. Piccinini (2016). Shear wave splitting of the 2009 L'Aquila seismic sequence: fluid saturated microcracks and crustal fractures in the Abruzzi region (Central Apennines, Italy), Geophys. J. Int., 204, 1531–1549.

Baccheschi, P., L. Margheriti and M.S. Steckler (2007). Seismic anisotropy reveals focused mantle flow around the Calabrian slab (Southern Italy), Geophys. Res. Lett., 34, L05302, doi:10.1029/2006GL028899, 2007.

Backus, G.E. (1962). Long-wave elastic anisotropy produced by horizontal layering, J. Geophys. Res., 67, 11, 4427–4440.

Barruol, G., P.G. Silver and A. Vauchez (1997). Seismic anisotropy in the eastern US: deep structure of a complex continental plate. J. Geophys. Res., 102, B4, 8329–8348.

Barruol, G. and R. Hoffmann (1999). Seismic anisotropy under the Geoscope stations, J. Geophys. Res., 104, B5, 10757–10773.

Bougrine, A., A. Yelles-Chaouche and E. Calais (2019). Active deformation in Algeria from continuous GPS measurements, Geophys. J. Int., 217, 572–588.

Bokelmann, G., E. Qorbani and I. Bianchi (2013). Seismic Anisotropy and Large-Scale Deformation of the Eastern Alps, Earth Planet. Sci. Lett., doi: 10.1016/j.epsl.2013.09.019.

Bowman, J.R. and M. Ando (1987). Shear-wave splitting in the upper-mantle wedge above the Tonga subduction zone, Geophys. j. R. Astron. Soc., 88, 25–41.

Bracène, R. and D. Frizon de Lamotte (2002). The origin of intraplate deformation in the Atlas system of western and central Algeria: from rifting to Cenozoic-Quaternary inversion, Tectonophysics, 357, 207– 226.

Calais, E., C. DeMets and J.M. Nocquet. (2003). Evidence for a post–3.16 Ma change in Nubia–Eurasia–North America plate motions, Earth Planet. Sci. Lett., 216, 81–92.

Christensen, N.I. and R.S. Crosson. (1968). Seismic anisotropy in file upper mantle, Tectonophysics 6, 93-107.

Civiero, C., S. Custódio, N. Rawlinson, V. Strak, G. Silveira, P. Arroucau and C. Corela (2019). Thermal nature of mantle up wellings below the Ibero-western Maghreb region inferred from teleseismic tomography, J. Geophys. Res., 124, 1781–1801. https://doi.org/10.1029/2018JB016531.

Crampin, S. (1984). Effective anisotropic elastic constants for wave propagation through cracked solids, Geophys. J. R. Astron. Soc., 76, 135–145.

Davis, J.C (1986). Statistics and Data Analysis in Geology, 2nd Edition, John Wiley, New York, 646.

DeMets, C., G. Iaffaldano and S. Merkouriev (2015). High–resolution Neogene and Quaternary estimates of Nubia–Eurasia–North America Plate motion, Geophys. J. Int., 203, 1, 416–427.

Diaz, J. and J. Gallart (2014). Seismic anisotropy from the Variscan core of Iberia to the Western Africa Carton: New constrains on upper mantle flow at regional scales, Earth Planet. Sci. Lett., 394, 48–57.

Díaz, J., J. Gallart, A. Villaseñor, F . Mancilla, A . Pazos, D . Córdoba, J.A. Pulgar, P. Ibarra and M. Harnafi (2010). Mantle dynamics beneath the Gibraltar Arc (western Mediterranean) from shear-wave splitting measurements on a dense seismic array, Geophys. Res. Lett., 37(L18304), doi:10.1029/2010GL044201.

Fichtner, A. and A. Villaseñor (2015). Crust and upper mantle of the western Mediterranean – Constraints from full-waveform inversion, Earth Planet. Sci. Lett., 428, 52-62.

Hamai, L., B. Petit Carole, L. Le Pourhiet, A. Yelles-Chaouche, J. Déverchère, M.O. Beslier and A. Abtout (2018). Towards subduction inception along the inverted North African margin of Algeria? Insights from thermo-mechanical models, Earth Planet. Sci. Lett., 501, P 13-23.

Houlie, N. and T. Stern (2012). A comparison of GPS solutions for strain and SKS fast directions: Implications for modes of shear in the mantle of a plate boundary zone, Earth Planet. Sci. Lett., 345–348, P 117-125.

Jolivet, L., R. Augier, C. Faccenna, F. Negro, G. Rimmele, P. Agard, C. Robin, F. Rossetti and A. Crespo-Blanc (2008). Subduction, convergence and the mode of backarc extension in the Mediterranean region, Bull. Soc. géol. Fr., 179 (6), 525–550.

Kendall, J.M., S. Pilidou, D. Keir, I. Bastow, G. Stuart and A. Ayele (2006). Mantle up wellings, melt migration and rifting in Africa: insights from seismic anisotropy, Geol. Soc. Spec. Publ., 259, 55–72.

Layadi, K., F. Semmane and A. Yelles-Chaouche (2016). Site-effects investigation in the city of Chlef (formerly El-Asnam), Algeria, using earthquake and ambient vibration data, Bull. Seismol. Soc. Am., 106, 2185–2196.

Levin. V., S. Roecker, P. Graham and A. Hosseini (2008). Seismic anisotropy indicators in Western Tibet: Shear wave splitting and receiver function analysis. Tectonophysics 462, 99-108.

Lemnifi, A.A.K.H., S.S. Liu, C.A. Gao, A.A. Reed, Y.Yu. Elsheikh, and A.A. Elmelade (2015). Azimuthal anisotropy beneath north central Africa from shear wave splitting analyses, Geochem. Geophys. Geosyst., 16, 1105–1114, doi:10.1002/2014GC005706.

Liu, J., J. Wu, W. Wang, L. Fang and C. Chang (2020). Seismic anisotropy beneath the eastern margin of the Tibetan Plateau from SKS splitting observations, Tectonophysics, 785, https://doi.org/10.1016/j.tecto.2020.228430.

Lucente, F.P., L. Margheriti, C. Piromallo and G. Barruol. (2006). Seismic anisotropy reveals the long route of the slab through the western-central Mediterranean mantle, Earth Planet. Sci. Lett., 241, 517-529.

Mainprice, D. (2007). Seismic anisotropy of the deep Earth from a mineral and rock physics perspective, In: Schubert, G. (Ed.), Treatise on Geophysics, 2, 437–492.

Mardia, K.V. and P.E. Jupp (2000). Directional Statistics, John Wiley, 429.

Margheriti. L., F.P. Lucente and I.S. Pondrell (2003). SKS Splitting measurements in the Appenninic-Tyrrhenian domains (Italy) and their relation with Lithospheric subduction and mantle convection, J. Geophys. Res., 108, B4, 2218.

Qorbani, E., I. Bianchi and G. Bokelmann (2015). Slab detachment under the Eastern Alps seen by seismic anisotropy, Earth Planet. Sci. Lett., 409, 0, 96–108, doi:10.1016/j.epsl.2014.10.049.

Peral, M., M. Fernandez, J. Vergés, S. Zotnik and I. Jiménez-Munt (2022). Numerical modelling of opposing subduction in the Western Mediterranean, Tectonophysics, S0040-1951(22)00103-2.

Radi, Z., A. Yelles-Chaouche and G. Bokelmann (2015). Seismic anisotropy of northeastern Algeria from shear-wave splitting analysis, Phys. Earth Planet. Inter., 248, 73–82.

Radi, Z., A. Yelles-Chaouche, V. Corchete and S. Guettouche (2017). Crust and upper mantle shear wave structure of Northeast Algeria from Rayleigh wave dispersion analysis, Phys. Earth Planet. Inter., 270, 84-89.

Radi, Z. and A. Yelles-Chaouche (2022). Shear velocity structure beneath Northern Algeria from Rayleigh-wave analysis, J. African Earth Sci., 186, 104446.

Schmid, C., S. Van der Lee and D. Giardini (2004). Delay times and shear-wave splitting in the Mediterranean region, Geophys. J. Int., 159, 275-290.

Silver, P.G. and W.W. Chan (1991). Shear wave splitting and subcontinental mantle deformation, J. Geophys. Res., 96, 16, 16.429–16.454.

Spakman, W. and R. Wortel (2004). A tomographic view on Western Mediterranean geodynamics, in The TRANSMED Atlas - The Mediterranean Region From Crust to Mantle, edited by W. Cavazza et al., 31–52, Springer, Berlin, Heidelberg.

Wang, C., L.M. Flesch, P.G. Silver, L. Chang and W.W. Chan (2008). Evidence for mechanically coupled lithosphere in central Asia and resulting implications, Geology, 36, 5, 363-366.

Wildi, W. (1983). La chaîne tello-rifaine (Algérie, Maroc, Tunisie): Structure, stratigraphie et évolution du Trias au Miocène, Revue de géographie physique et de géologie dynamique, 24, 201-297.

Wüstefeld, A. and G. Bokelmann. (2007). Null detection in shear-wave splitting measurements, Bull. Seismol. Soc. Am., 97, 4, 1204–1211.

Wüstefeld, A., G. Bokelmann, C. Zaroli and G. Barruol (2008). SplitLab: a shear-wave splitting environment in Matlab, Comput Geosci., 34, 5, 515–528.

Yelles-Chaouche, A., T. Allili, A. Alili, W. Messemen, H. Beldjoudi, F. Semmane, A. Kherroubi, H. Djellit, Y. Larbes, S. Haned, A. Deramchi, A. Amrani, A. Chouiref, F. Chaoui, K. Khellaf and C. Nait Sidi Said (2013). The new Algerian Digital Seismic Network (ADSN): towards an earthquake early-warning system, Advances in Geosciences., 36, 31-38.

Zhao, L., T.Y. Zheng, L. Chen and Q.S. Tang (2007). Shear wave splitting in eastern and Central China: implications for upper mantle deformation beneath continental margin, Phys. Earth Planet. Inter., 162, 73–84.

***CORRESPONDING AUTHOR: Zohir RADI**,
Center of Research in Astronomy Astrophysics and Geophysics, Algiers Algeria
e-mail: zohiradi34@yahoo.fr